Bioactive Materials 20 (2023) 1–15

Contents lists available at ScienceDirect

Bioactive Materials

journal homepage: www.keaipublishing.com/en/journals/bioactive-materials

Canine ACL reconstruction with an injectable hydroxyapatite/collagen paste for accelerated healing of tendon-bone interface

Qingsong Jiang [a,1], Liren Wang [b,1], Zhanhong Liu [a,1], Jinlei Su [a], Yajun Tang [a], Peijie Tan [a], Xiangdong Zhu [a], Kai Zhang [a], Xing Ma [c], Jia Jiang [b], Jinzhong Zhao [b,**], Hai Lin [a,*], Xingdong Zhang [a]

[a] National Engineering Research Center for Biomaterials, Sichuan University, 29 Wangjiang Road, Chengdu, Sichuan, China
[b] Department of Sports Medicine, Shanghai Jiao Tong University Affiliated Sixth People's Hospital, 600 Yishan Road, Shanghai, China
[c] Department of Orthopaedics, First Affiliated Hospital of Xi'an Jiaotong University, 277 West Yanta Road, Xi'an, Shaanxi, China

ARTICLE INFO

Keywords:
Anterior cruciate ligament reconstruction
Tendon-bone healing
Injectable paste
Hydroxyapatite
Collagen

ABSTRACT

Healing of an anterior cruciate ligament (ACL) autologous graft in a bone tunnel occurs through the formation of fibrovascular scar tissue, which is structurally and compositionally inferior to normal fibrocartilaginous insertion and thus may increase the reconstruction failure and the rate of failure recurrence. In this study, an injectable hydroxyapatite/type I collagen (HAp/Col I) paste was developed to construct a suitable local microenvironment to accelerate the healing of bone-tendon interface. Physicochemical characterization demonstrated that the HAp/Col I paste was injectable, uniform and stable. The *in vitro* cell culture illustrated that the paste could promote MC3T3-E1 cells proliferation and osteogenic expression. The results of a canine ACL reconstruction study showed that the reconstructive ACL had similar texture and color as the native ACL. The average width of the tunnel, total bone volume, bone volume/tissue volume and trabecular number acquired from micro-CT analysis suggested that the healing of tendon-bone interface in experimental group was better than that in control group. The biomechanical test showed the maximal loads in experimental group achieved approximately half of native ACL's maximal load at 24 weeks. According to histological examination, Sharpey fibers could be observed as early as 12 weeks postoperatively while a typical four-layer transitional structure of insertion site was regenerated at 48 weeks in the experimental group. The injectable HAp/Col I paste provided a biomimetic scaffold and microenvironment for early cell attachment and proliferation, further osteogenic expression and extracellular matrix deposition, and *in vivo* structural and functional regeneration of the tendon-bone interface.

1. Introduction

Anterior cruciate ligament (ACL) plays an essential role in maintaining the normal movement and stability of knee joint. The injury of ACL leads to abnormal joint kinematics, and secondary structural damage of articular cartilage and meniscus, which result in chronic degenerative joint changes [1–3]. Injured ACL has a limited capacity of self-regeneration, thus surgical reconstruction is always necessary, especially when the ligament is ruptured [1]. ACL reconstruction with autologous grafts is one of the main therapies in current clinic, while the grafts include semitendinosus and gracilis tendons, bone-patellar tendon-bone (BPTB) graft, hamstring tendon [4–6]. BPTB graft was once the gold standard due to the achieved bone-bone healing in the bone tunnels. Lately hamstring tendon is becoming the most common graft applied in the orthopaedic community [6–8] because significant complications such as donor pain, quadriceps atrophy and flexion contracture were reported in BPTB therapy [9,10].

Although great improvements have been achieved in ACL reconstruction with autologous grafts, limitations and challenges are still remaining. The major disadvantages of autologous grafts therapy include the comparatively long tendon-bone healing time and unpredictable healing results [11,12]. More importantly, the actual healing in

Peer review under responsibility of KeAi Communications Co., Ltd.
* Corresponding author. National Engineering Research Center for Biomaterials, Sichuan University, Chengdu, Sichuan, China.
** Corresponding author.
E-mail address: linhai028@scu.edu.cn (H. Lin).
[1] These authors contributed equally.

https://doi.org/10.1016/j.bioactmat.2022.05.003
Received 8 January 2022; Received in revised form 1 May 2022; Accepted 2 May 2022
Available online 17 May 2022

bone tunnels is driven by the formation of fibrovascular scar tissue which is structurally and compositionally inferior to native tissue [13,14]. As a consequence, this fibrous tissue exposes the insertion site to high mechanical stress which may increase the reconstruction failure and the rate of failure recurrence [15–17], leading to further efforts to enhance and accelerate tendon-bone healing.

The ideal tendon-bone healing is the restoration of native interface structure and rehabilitation of tendon/ligament anchoring function. The native interface of tendon/ligament to bone is a specialized tissue known as "enthesis", which integrates the ligament in bone and facilitates the dissipation of stresses across the interface. This direct insertion site contains four distinct types of tissue: ligament, uncalcified fibrocartilage, calcified fibrocartilage and bone [18–20]. However, these distinctive tissues contain similar extracellular matrix (ECM) which primarily consists of type I collagen (Col I), mineral component (~99% hydroxyapatite) and small amounts of proteoglycans [16,17]. A strong mechanical attachment between ligament and bone is established *via* a compositional and structural gradient in the ECM.

In recent research, many interventions such as mechanical stimulation [21], tendon wrapping with periosteum [22], growth factors [23], bone marrow stromal cells [24], gene transfer [25] and bone substitute materials [26,27] were applied to achieve better tendon-bone healing. However, previous experimental studies have shown that the structure and function of normal ACL insertion sites have not been ideally replicated after ACL reconstruction [28,29].

Based on the principles of "tissue-inducing biomaterials" theory, a strategy of developing biomimetic biomaterial was utilized in this study to prepare and evaluate an injectable paste with optimized materials' parameters to promote tendon-bone interface regeneration and facilitate functional rehabilitation. Such injectable paste is composed of hydroxyapatite particles (HAp) [30] and type I collagen (Col I) [31], which were both widely used in Food and Drug Administration cleared implantable devices. HAp is a natural mineral compound that is often used as bone void fillers, bone graft substitutes and implant coatings to promote the growth of new bone [32,33]. As the main organic composition in ECM of many tissues, Col I provides suitable microenvironments for cells such as fibroblasts, osteoblasts and BMSCs, and also plays an important role in regulating cell behaviors including adhesion, proliferation and differentiation [34–38]. Both HAp and Col I possessed the characteristics which were beneficial to the regeneration of tendon-bone healing during the ACL reconstruction, and therefore they were used as raw materials for the injectable paste in this study.

The injectable Hap/Col I paste was prepared with optimized materials parameters, including the collagen concentration, particle size of HAp, and composition ratio of HAp, and then undergone systematic *in vitro* and *in vivo* evaluation. Particularly, the physicochemical properties of HAp/Col I paste were characterized, including injectability, uniformity and stability. In addition, the cellular response of HAp/Col I paste was studied. Finally, the HAp/Col I paste was evaluated in a canine ACL reconstruction model to investigate its effect to promote the tendon-bone healing process as well as to regenerate the tendon-bone interface structurally and functionally.

2. Materials and methods

2.1. Materials

Type I collagen was extracted and purified from newborn calfskin in our laboratory. Calcium nitrate tetrahydrate ($Ca(NO_3)_2{\cdot}4H_2O$), ammonium phosphate ($(NH_4)_2HPO_4$), aqueous ammonia (NH_4OH), acetic acid (HAC) and sodium hydroxide (NaOH) were purchased from Kelong Reagent Company (Chengdu, China). α-Minimum Essential Medium (α-MEM, Hyclone) and Fetal bovine serum (FBS, Gibco, Australia origin) were purchased from Thermo Fisher Scientific Corporation (USA). Fluorescein diacetate (FDA), propidium iodide (PI), rhodamine phalloidin and 4′,6-diamidino-2-phenylindole (DAPI) were purchased from Sigma-Aldrich (USA). All chemicals were used as received without further treatment unless otherwise stated.

2.2. Preparation and characterization of HAp/Col I pastes

Spherical HAp particles were prepared by a two-step process including wet precipitation and spray drying. Briefly, 1.0 mol/L diammonium phosphate ($(NH_4)_2{\cdot}HPO_4$) solution was added gradually into 1.0 mol/L calcium nitrate ($Ca(NO_3)_2{\cdot}4H_2O$) solution according to the molar ratio of Ca/P = 1.67. The pH of the reactive system was adjusted to around 10.0 by aqueous ammonia (NH_4OH) and the reaction temperature was set at 70 °C. After reaction for 4 h, the slurry obtained was aged for 24 h and then washed with distilled water for 3 times. The spherical HAp particles were produced by spray-drying the slurry with a SFDC-20 Spray Dryer (Shanghai Ohkawara Dryers Co., China), and the particles within specific size range (40–71 μm) were further sieved and collected. The final attained HAp particles were sterilized by dry heat at 300 °C for 2 h. On the other hand, self-prepared type I collagen (Col I) was extracted from calfskin by pepsin and dissolved in 0.5 mol/L acetic acid (HAC) to a concentration of 10 mg/mL. The collagen was treated by chemical sterilization and followed the sterility process control protocol during the preparation. The pH of the collagen solution was adjusted to 7.2–7.4 by adding 2 mol/L sodium hydroxide (NaOH) solution in an ice bath. Finally, the HAp/Col I pastes were prepared by aseptic processing with blending sterilized HAp particles with Col I solution (10 mg/mL) to 40 wt% directly under stirring (T10, IKA, Germany) for 5 min, which was carried out in an ice bath. Then, the HAp/Col I paste was transferred into syringes (1 mL) and degassed by centrifugation at RCF of 1775g for 30 s (D-37520, Sigma, Germany). The as-prepared samples were stored at 4 °C for further study.

The physical properties of HAp/Col I pastes such as composition, structural morphology and uniformity, systematical stability and injectable performance were characterized. The compositions of the HAp/Col I paste were analyzed by a thermal gravimetric analyser (TG 209 F3, Netzsch) at a heating rate of 10 °C/min from 25 °C to 600 °C in flowing air. To study its microstructure, the HAp/Col I paste was firstly frozen in liquid nitrogen and lyophilized to obtain the samples for scanning electron microscopy (SEM, HITACHI S-800, Japan) analysis. The cross-sections of the test samples were prepared and further sputter-coated with a layer of gold. The energy dispersive spectroscopy (EDS) mapping for Ca, P and C elements was implemented to study the distribution of inorganic particles in the composite.

To evaluate the compositional uniformity, HAp/Col I paste was gently extruded into a cylindrical mold with a diameter of 8 mm and a height of 2.5 mm, and immediately frozen at −20 °C to stabilize the distribution of compositions in the paste. Then the frozen samples were embedded in O·C.T Compound (SAKURA Tissue-Tek, USA) and sliced to 5 μm thick sections by a cryostat (Leica CM1850, Germany). Following the staining by Alizarin Red S, the sections were imagined to observe the composition distribution. In addition, the porosity of the paste could be estimated by area analysis of the pore zone and the matrix zone using Image J 1.8.0.

The systematical stability of HAp/Col I paste was assessed by both macroscopic observation and elements release analysis during and after the sample extraction. Briefly, the HAp/Col I paste was extruded from the syringe into a petri dish to form a word "HA" in saline according to the extraction ratio in ISO 10993–12 [39]. After soaking for 7, 14 and 28 days at 37 °C, the macroscopic morphologies were recorded and the concentrations of released Ca and P were determined by inductively coupled plasma-atomic emission spectrometer (ICP-OES, Varian 700-ES, USA).

For injectability performance evaluation, the paste was filled in 1 mL syringe equipped with an 18-gauge needle (1.2 mm of inner diameter) and then extruded by a vertical compressive load on the top of syringe plunger. The experiments were performed on a universal material testing machine (AGS-X, SHIMADZU, Japan) at a constant speed of 30

mm/min. The curve of the pushing force against piston displacement was recorded. All samples were analyzed in triplicate.

2.3. In vitro cell culture

2.3.1. Culture of MC3T3-E1

MC3T3-E1 preosteoblasts were purchased from National Collection of Authenticated Cell Cultures (Chinese Academy of Sciences, Shanghai, China). Cells were cultured in α-MEM (HyClone, USA) supplemented with 10% fetal bovine serum (FBS, Gibco, Australia) and 1% antibiotic/antimycotic (HyClone, USA). Cells were grown in a humidified atmosphere of 5% CO_2 at 37 °C. When reaching 70–80% confluence, adherent cells in dishes (Costar, USA) were harvested and passaged. The third-passage cells were used in the co-culture process.

2.3.2. Cell viability, proliferation and morphology

The MC3T3-E1 preosteoblasts and HAp/Col I paste were uniformly mixed to a cell density of 2×10^6 cells/mL in sterile environment using a hand-held homogenizer (T10, IKA, Germany). 0.25 mL MC3T3-E1 preosteoblasts-loaded paste was carefully transferred into self-prepared cylindrical molds (diameter: 8 mm, height: 2.5 mm) with 1 mL syringe. The gelation of the cells/paste constructs could be finished in 30 min and the samples were further incubated at 37 °C for 24 h and separated from the molds for further culture. Since there was no launched product for similar indication or composite with similar characterization, no suitable control group was applied in the *in vitro* cell culture process. Each well of ultralow adhesive 24-well plate (Costar, USA) received one sample and 2 mL culture media. The samples were cultured under identical conditions (5% CO_2, 37 °C) for 2 weeks and the culture media was changed every 2 d. After culturing for 1, 3, 7 and 14 d, fluorescein diacetate (FDA) and propidium iodide (PI) molecule probes were used to investigate the viability of MC3T3-E1 preosteoblasts. Briefly, the cultured samples were rinsed with PBS three times and immersed in PBS solution containing 1 μg/mL of FDA and 1 μg/mL of PI for 5 min before the observation with confocal laser scanning microscope (CLSM, ZEISS LSM 880, Germany). Meanwhile, the cell proliferation was evaluated at the same time intervals by cell counting KIT-8 (CCK-8) according to the instructions from the manufacturer. Following the harvest of cell/paste constructs, they were incubated in 10% (v/v) CCK-8 solution for 4 h at 37 °C and 5% CO_2. 100 μL of the supernatant was transferred to a new 96-well plate to be determined at 450 nm using a microplate reader (Varioskan Flash, Thermo Flasher Scientific, USA).

At the given culture time points, the morphology of cells in cell/paste constructs was examined with F-actin fluorescence staining and SEM. For F-actin fluorescence staining, samples were washed with PBS and fixed in 4% (w/v) paraformaldehyde for 30 min at 4 °C, permeated with 0.25% (v/v) Triton X-100 (Sigma-Aldrich, USA) for 10 min at 25 °C, and then washed using PBS for three times. Finally, these samples were stained with rhodamine-phalloidin solution (5 μg/mL, Sigma-Aldrich) for 6 h and with DAPI (10 μg/mL, Sigma-Aldrich) for 2 min at 25 °C. Subsequently, the constructs were rinsed with PBS and photographed using a CLSM. For SEM observation, samples were fixed in 2.5% (w/v) glutaraldehyde solution for 48 h at 4 °C, and then dehydrated with a gradually increasing ethanol concentration of 30, 50, 70, 90, 95 and 100% (v/v) for 30 min at each step. The samples were dried using a critical point dryer (Leica EM CPD300, Germany) and observed with SEM after coating with gold in an ion sputter.

2.3.3. Evaluation of osteogenic properties

After being *in vitro* cultured for 7 and 14 d, the cell/paste constructs were collected and frozen at −20 °C in RNAlater® solution (Ambion) for further RNA extraction and expression test. Rneasy® Mini Kit (Qiagen) was applied to extract the RNA and the concentration was measured by microspectrophotometer (ND1000, Nanodrop Technologies). Then, the RNA expression of alkaline phosphatase (ALP), bone morphogenetic protein (BMP-2), osteocalcin (OCN), osteopontin (OPN) and runt related transcription factor 2 (Runx-2) genes was determined by reverse transcription-polymerase chain reaction (RT-PCR) while GAPDH was used for normalization and primers were listed in Table 1 [40]. PCR was performed at 94 °C for 45 s, 60 °C for 45 s, and 72 °C for 1 min, for 30 cycles. The PCR products were analyzed on 1% (w/v) agarose gel and stained by ethidium bromide. The transcription level normalized to GAPDH was calculated using the 2^{Δ}Ct formula.

2.4. In vivo evaluation of HAp/Col I paste

2.4.1. Surgical procedure

The animal study was approved by the Ethical Committee of Sichuan University. A total of 36 male mature beagle dogs weighing 11.55 ± 1.08 kg were used for *in vivo* evaluation of HAp/Col I paste. The dogs were reared according to the guidelines of the ethical committee and the National Institutes of Health guidelines for the care and use of laboratory animals. The dogs were randomly assigned into two groups (i.e., experimental and control groups) and were fed 7 d to adapt to the environment before the surgery. Unilateral ACL injury model was established in all dogs and further undergone surgical reconstruction, which had a diagram shown as Fig. S1. The procedures were displayed as Fig. S2 and went briefly as following. Firstly, intravenous anesthesia with pentobarbital sodium (30 mg/kg, body weight) was administered. Then, the peroneus longus tendon was identified and then removed as a transplant donor through a 1 cm incision which was made along the posterior side of the distal tibia. The acquired tendon segment of approximate 8 cm long was folded in half to create a double-strand ACL graft and both ends were sutured with one No. 2 polyester suture (Ethibond; Ethicon, Somerville, NJ) in a whip-stitch style. The proximal end of the graft was trimmed to yield a diameter of 4.5 mm. Through an anteromedial incision and a medial parapatellar arthrotomy, the knee joint cavity was exposed. The native ACL was excised at its femoral and tibial origins. In a surgical position of 70°–90° knee flexion, femoral and tibial tunnel was constructed *via* a drilling point between the medial tibial tubercle and the medial edge of the tibia by a 1.5 mm Kirschner needle along the direction of tibial trochanter-anterior cruciate ligament tibial end-anterior cruciate ligament femoral end-femur. Then, 4.5 mm hollow drill was used to enlarge the bone tunnel. Following the injection and fully filling of the paste, the pre-stretched and wetted graft was implanted into bone tunnel. The plate was fixed at the external entrance of the femoral tunnel and the polyester suture drawn from the tibial tunnel was fixed as a stake below the external entrance of the tibial tunnel. Following the immobilization of implants, the joint cavity was completely washed with saline to remove any remain. Finally, the joint cavity was closed and sutured as shown in Fig. S2L. In the control group, no additional biomaterial was implanted between graft and bone tunnel. After the surgery, the animals were kept in individual cages for free movement at room temperature on a 12 h light/dark cycle. Standard balanced food and water were available for freely intake. Intramuscular injection with penicillin (250 kU/kg) and streptomycin (80 mg/kg) was administered every day for the first 3 postoperative days. The dogs were

Table 1
Primer sequences for the Real Time RT-PCR analysis.

Gene	Primer sequences
GAPDH	Forward: CAGTGGCAAAGTGGAGATTGTTG
	Reverse: TCTCGCTCCTGGAAGATGGTGAT
ALP	Forward: ATCTTTGGTCTGGCTCCCATG
	Reverse: TTTCCCGTTCACCGTCCAC
BMP-2	Forward: TCTTCCGGGAACAGATACAGG
	Reverse: TGGTGTCCAATAGTCTGGTCA
Runx-2	Forward: ATGCTTCATTCGCCTCACAAA
	Reverse: GCACTCACTGACTCGGTTGG
OCN	Forward: CTCCCATTGGCGAGTTTG
	Reverse: TGTAGTCCAGGTGGAGCTTGTG
OPN	Forward: ACACTTTCACTCCAATCGTCCCTAC
	Reverse: GGACTCCTTAGACTCACCGCTCTT

sacrificed at 12, 24 and 48 weeks for microcomputed tomography (micro-CT), histologic examination and biomechanical testing.

2.4.2. General observation and harvest procedure

All the animals were daily inspected on surgical site after the operation, including the wound healing, infection situation and knee movement, to have an initial evaluation of ACL reconstruction. The animals were sacrificed at 12, 24 and 48 weeks postoperatively in both experimental and control groups by intravenous administration of a pentobarbital overdose (100 mg/kg). After the sacrifice, the knee joint cavity was exposed following the separation of subcutaneous tissue and medial retinaculum, and the dislocation of patella along a cut on the medial edge of the patella. The mobility of the joint, integrity of the graft, the condition of articular cartilage and meniscus were observed. The distal femur, proximal tibia and the soft tissues in between were all harvested for further detection. The reconstructive ACL of both groups were sampled for hematoxylin and eosin (HE) staining to have a histological analysis. Also, the reconstructive ACL were sampled and the morphology was further examined with SEM after fixing in 10% (w/v) formalin for 48 h and drying by a critical point dryer.

2.4.3. Microcomputed tomography (micro-CT) analysis

For quantifying the ingrowth of mineralized tissue inside the bone tunnel, micro-CT analysis was performed using a high-resolution micro-CT system (VivaCT80, SCANCO Medical AG). Three samples (n = 3) from each group were harvested for micro-CT analysis at the given time. The parameters were set with the energy of 80 kV, the intensity of 450 μA, the isotropic resolution of 20 μm and the optimal threshold value of 300. The scanning direction was perpendicular to the long axis of the sampled bone tissue, covering the entry and exit of the bone tunnel. A customized cylindrical region of interest (ROI) (diameter: 10 mm, height: 7 mm) containing the bone tunnel was chosen to quantitatively analyze the newly formed mineralized tissue over time. Based on the ROI of sample which was reconstructed using Materialise Mimics V17.0 software, the total bone volume (TBV, mm^3), bone volume fraction (BV/TV, %), trabecular number (TbN, 1/mm) of mineralized tissue inside the tendon-bone interface was calculated and elucidated. The average tunnel diameter was measured using the axial images of the sampled femoral and tibial bone tissue.

2.4.4. Histological analysis

After micro-CT analysis, the ACL-bone complexes (n = 3) from each group were fixed in 10% (w/v) neutral buffered formalin for 7 days, dehydrated with graded alcohol of 70, 80, 90, 95 and 100% (v/v) for 12 h at each step, then cleaned by dimethylbenzene and embedded in polymethyl methacrylate (PMMA, Technovit 9100, Germany). The embedded samples were sectioned by saw microtome (2500E, Leica, Germany) and the slicing direction was parallel to the long axis covering the entry and exit of the bone tunnel. Then, the sections were cut, grinded and polished to 5 μm (Exakt Micro-Grindin System, Leica, Germany) and stained with hematoxylin and eosin (HE), masson trichrome staining (Masson) to have a histological analysis.

2.4.5. Biomechanical test

The biomechanical properties of the retrieved implants were tested following the previously established protocol. Before the test, the retrieved implants which were frozen and preserved at −80 °C were slowly thawed at 4 °C, and all soft tissue except for the regenerated ligament was removed to attain test samples of femur-graft-tibia complex. Four samples (n = 4) from experimental and control groups were used and another four native femur-ACL-tibia complexes were served as normal control. The femur and tibia were immobilized with specially designed clamps at both ends, allowing tensile loading along with the long axis of the graft in a testing machine (AGS, Shimadzu Corporation, Japan). The test was performed at a constant rate of 10 mm/min, and the ultimate failure loads were recorded. All samples were kept moist with phosphate buffered saline (PBS) solution during the test.

2.5. Statistical analysis

Statistical analysis was performed using one-way analysis of variance (ANOVA) followed by Tukey's posthoc testing using SPSS 22.0 software. These data were presented as mean ± standard deviation (SD). The significance level was set at $p < 0.05$ (*), $p < 0.01$ (**), $p < 0.001$ (***).

3. Results

3.1. Physical characterization of HAp/Col I paste

The as-prepared HAp/Col I paste which was filled in the syringe showed coherence and milk-white color (Fig. 1A). The TGA curves of the pastes suggested a sharp decline owing to the water evaporation till 120 °C as the peak end temperature shown in differential curves (DTG), and a slight decline before 350 °C because of the thermal decomposition of collagen. Finally, the thermally stable contents were 40.64% ± 0.39% which attributed to the HAp particles (Fig. 1B). The average diameter of spherical HAps calculated through Image J software (version 1.8.0) was 54.82 ± 1.18 μm (Fig. 1C), which was at the center of a normal distribution. The SEM image of the cross-section of lyophilized paste was shown as Fig. 1D, which displayed a uniform distribution of spherical HAps in Col I and irregular interconnecting pores with average pore size of 30–80 μm. At higher magnification (Fig. 1E and F), the spherical HAp was composed of loosely structured nano-scale particles (30–100 nm).

The EDS mappings of element Ca (blue), P (green) and C (red) were shown as spots dispersed in HAp/Col I paste (Fig. 2A–C), and the overlapping of Ca, P and C further testified the uniform dispersion of inorganic particles and collagen carrier (Fig. 2D). Alizarin Red S staining images indicated that the HAp particles shown in red were homogeneously dispersed in collagen solution and no obvious particle aggregation was observed (Fig. 2F and G).

The staining result was consistent with those of SEM observation and EDS mappings. After immersing in the saline for 7, 14 and 28 d, the "HA" letters formed by HAp/Col I paste extruded from the syringe was stable and kept its original shape without any disintegration, which could be beneficial for surgical operation (Fig. 2H). The ICP-OES results suggested the HAps in the paste were stable and only 0.74%–2.11% were released and dissolved, which was estimated according to the Ca and P concentrations and changes in the extraction solutions (Fig. 2 I).

The compressive test illustrated that the loading force-displacement curves were smooth and showed analogous pattern among parallel samples. The loading force increased dramatically to initial the injection, followed by a linear increase and then achieved a relative stable level till all the paste was pushed out from the syringe. The average push-out forces of stable extrusion was 4.26 ± 0.28 N. (Fig. 2J).

3.2. In vitro cell culture

3.2.1. Cell viability, proliferation and morphology

Cell viability observed by CLSM and proliferation result determined by CCK-8 was shown in Fig. 3. The live/dead staining images indicated living cells were uniformly distributed in the pastes. Also, the green fluorescence intensity continuously increased with extending culture time, and only few of dead cells were detected, which meant cells encapsulated in the paste having good viability and proliferation (Fig. 3A). In addition, according to the results acquired from CCK-8 assay, the cell number in the pastes increased significantly from 1 to 14 d, which was consistent with the CLSM observation (Fig. 3B).

The cytoskeletal staining and SEM results of MC3T3-E1 preosteoblasts-loaded in paste were given in Fig. 3C. The F-actin and nucleus (blue) staining of preosteoblasts cytoskeleton demonstrated the cells quickly adhered to the matrix in the paste and cell spreading was observed at the initial stage of co-culture. Complete and well-spread

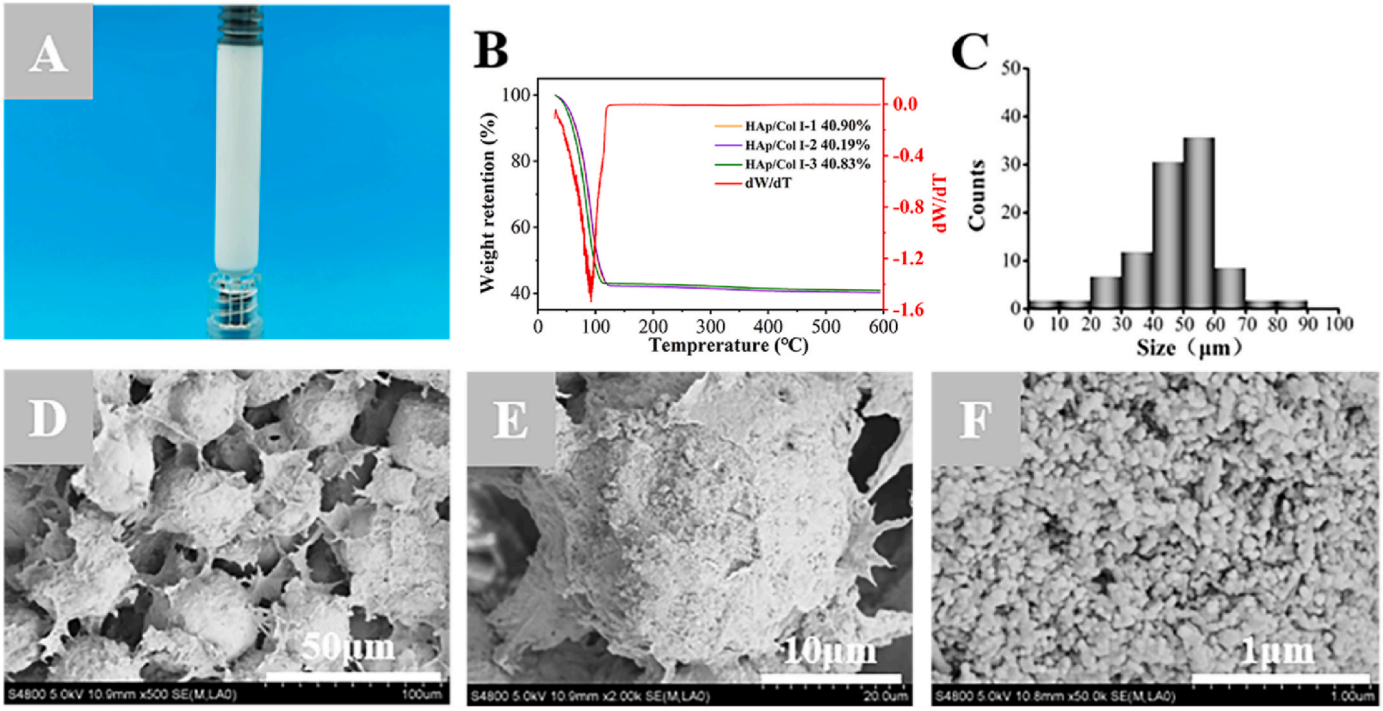

Fig. 1. The structural morphology and compositional contents of HAp/Col I paste. (A) The appearance of HAp/Col I paste loaded in syringe. (B) TGA and DTG curves of HAp/Col I pastes. (C) The size distribution of HAp particles. (D–F) SEM images of HAp/Col I paste at different magnifications.

morphology was seen after 7 d. The nuclei of MC3T3-E1 preosteoblasts were also observed to have normal morphology and well-defined actin filament. The SEM images of cell morphology and cell distribution were consistent with the F-actin and nucleus staining (Fig. 3C). The spreading area of individual cell at different time points was calculated using Image J, and the results showed that spreading area increased gradually and the whole visual field was covered at 14 d (Fig. 3D).

3.2.2. Osteogenic gene expression

The expression of five representative osteogenic genes, namely ALP which was a widely recognized marker of osteoblast differentiation, Runx2 which was an early marker of osteogenic maturation, OPN which was a later marker of osteogenic differentiation and mineralization, BMP-2 and OCN were measured to assess the osteogenic performance of MC3T3-E1 preosteoblasts using RT-PCR and the results were shown in Fig. 3E. Accordingly, it could be seen that the expressions of ALP and BMP-2 were nearly two times as other gene expressions after cultured for 7 d. After cultured for 14 d, the expressions of five genes were all up-regulated compared to those acquired at 7 d, while OPN was the only gene expression increased insignificantly ($p > 0.05$). In addition, ALP and BMP-2 were still the comparatively high expression genes among the five osteogenic genes, which were about twice higher than those of OCN and OPN.

3.3. In vivo animal study

3.3.1. General observation

All the animals had normal intakes and behavior post-operation. The body weight of each animal increased gradually and showed insignificant differences among groups (data not shown). No wound infection or accidental death occurred during the observation period. Except for two cases of joint instability caused by ligament absorption from the control limbs at 12weeks and 24 weeks respectively, the anterior drawer test and Lachman test yielded negative findings in the rest of knees. There was no obvious joint degeneration, effusion, or graft necrosis.

After the exposure of the implanted site, both grafts in the control and HAp/Col I groups were intact and had the similar texture and color as native ACL (Fig. 4A). Therein, the surface of the grafts was covered by a thin synovium-like tissue which probably secreted and formed owing to inflammation and especially obvious in the control group. H.E. staining results showed the collagen fibers in reconstructive graft were closely organized and arranged in parallel, which was similar to native ACL at 12, 24 and 48 weeks postoperatively (Fig. 4B, C, D). The oval and round fibroblasts were distributed among the collagen bundles and arranged in succession. Similarly, the SEM images displayed that the morphology of collagen bundles in reconstructive ACL was comparable with that in native ACL, including collagen bundle diameters, parallel ripple and spiral coiling modes (Fig. 4E, F, G), while the former collagen bundle tightness seemed inferior to that of latter.

Compared with the outcome at 12 weeks, the grafts in the experimental and control group seemed further matured at 24 and 48 weeks, and the ACL reconstruction could be considered to enter a stable ligamentation period based on their morphology and structure. According to the morphological characteristics, the shaping process of the transplanted graft could be divided into four stages: the early shaping stage, the shaping stage, the mature stage and the static stage. It was reported that the shaping and stabilization period of the graft was 26–36 weeks post-operation, which featured with regularly and evenly arranged collagen fibers in compact bundles and obviously co-directional ripples [41–43]. Furthermore, the tissue was mainly composed of oval-shaped cells, with fewer polygonal or star-forming shape [44].

3.3.2. Micro-CT analysis

The newly regenerated bone tissue within bone tunnels of femur and tibia was evaluated by micro-CT scan in both groups, and the results were shown in Fig. 5. Three-dimensional reconstruction images showed that the femoral and tibial tunnels in both experimental and control group contracted to a certain extent and the internal tunnel surface were uneven due to the growth of new bone tissue. Meanwhile, the entrance size of the femoral tunnel tended to be larger than that in the interior. The contraction of bone tunnel in the experimental group was more obvious than that in control group at each time point (Fig. 5A). The

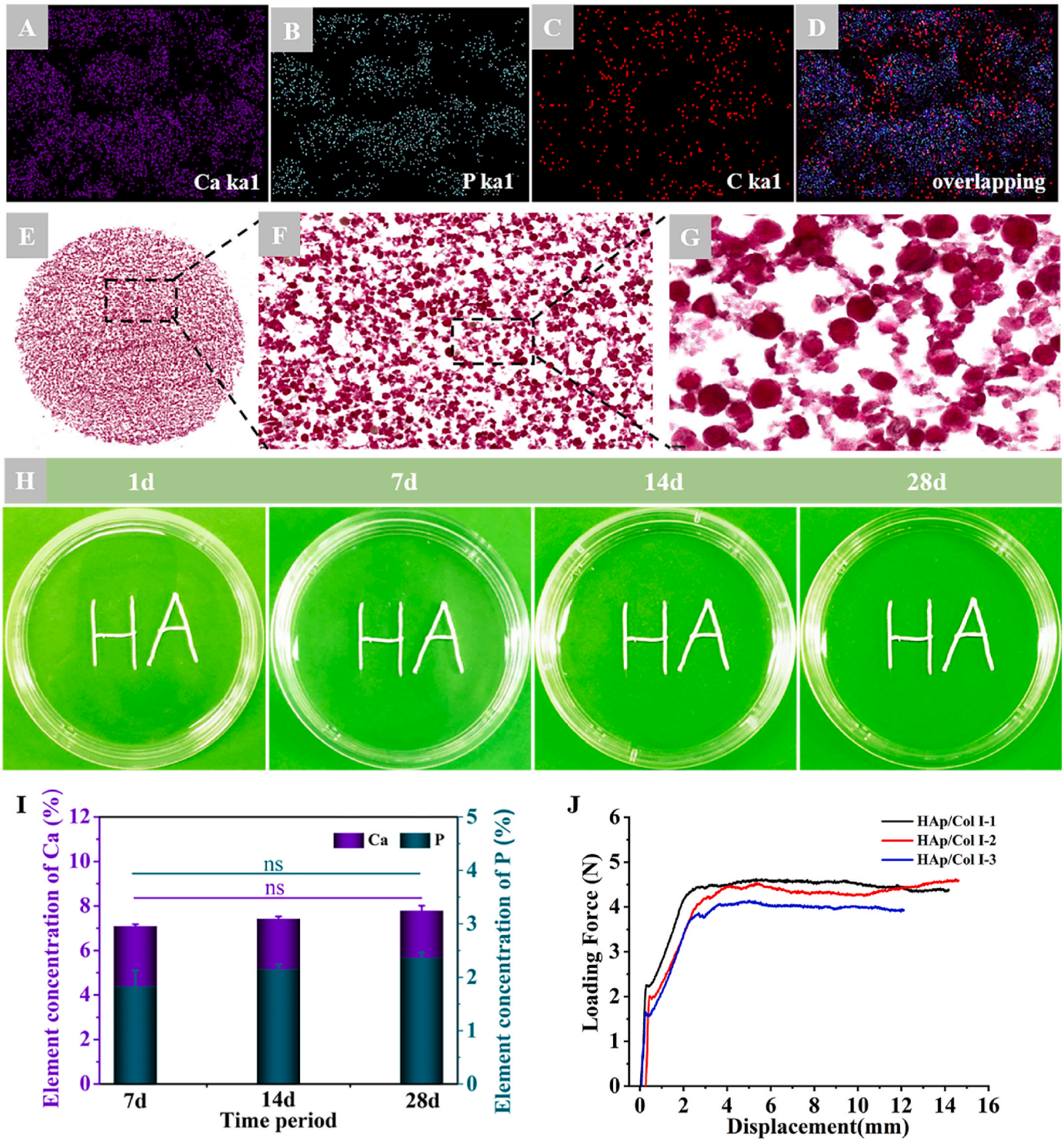

Fig. 2. The uniformity, systematical stability and injectable performance of HAp/Col I pastes. (A–D) EDS mapping results of Ca, P and C in HAp/Col I paste. (E–G) Alizarin Red S staining of HAp/Col I paste (E: × 10, F: × 100, G: × 200); (H) The macroscopic observation of HAp/Col I paste immersed in saline; (I) The contents of Ca and P element released into the extraction solution. (J) The loading force-displacement curves of HAp/Col I pastes extruding from the syringe.

average width of tibial and femoral tunnels was statistically analyzed and shown in Fig. 5B. Accordingly, the average width of the bone tunnels in the experimental group was significantly smaller than that in the control group at 12, 24 and 48 weeks. There was no significant change of average tunnel width from 24 weeks to 48 weeks in both groups. In addition, the tunnel width of tibia was smaller than that of femur in the same group (Fig. 5B).

Accordingly to the quantitative analysis results included the total bone volume (TBV), bone volume/tissue volume (BV/TV) and trabecular number (TbN) which were acquired based on the micro-CT reconstruction data, there was a significantly increasing trend of TBV, BV/TV and TbN in both femoral and tibial tunnels in experimental group from 12 weeks to 24 weeks (Fig. 5C, D, E). Typically, in experimental group, the level of BV/TV significantly increased from 26.5% ± 5.7% (12 weeks) to 33.8 ± 1.5% (24 weeks) in femur and 29.5% ± 1.8% (12 weeks) to 35.6% ± 2.8% (24 weeks) in tibia. In comparison, the data in

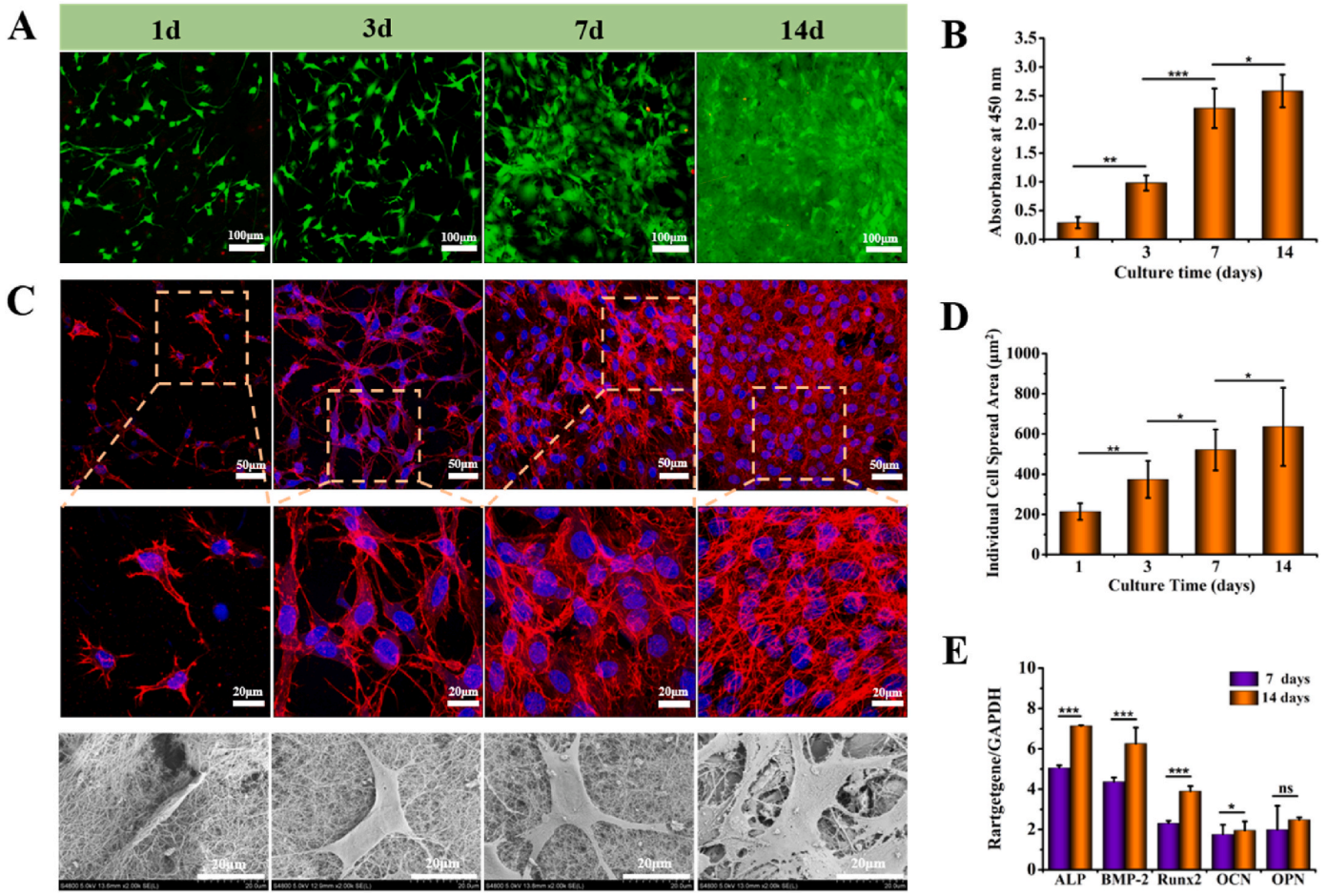

Fig. 3. Viability, proliferation and morphology of cells cultured in HAp/Col I paste. (A) Viability of MC3T3-E1 in HAp/Col I paste evaluated by confocal microscope (FDA/PI staining; green: live cells; red: dead cells). (B) Proliferation of MC3T3-E1 in HAp/Col I paste evaluated by CCK-8 assay (n = 6). (C) Morphology of MC3T3-E1 in HAp/Col I paste observed by F-actin fluorescence staining and SEM. (D) Spread area of individual cell *via* quantitative analysis (n = 12). (E) ALP, BMP-2, Runx2, OCN and OPN genes expression on 7 and 14 days. All results were normalized to the expression of GAPDH levels (n = 6).

the control group showed no significant difference at different time points and they were all significantly lower than those in the experimental group over the same period (Fig. 5D). In addition, the comparison between femoral and tibial data indicated that the bone tunnel healing in tibia was always superior to that in femur in both groups. Taking all results of 3D reconstruction and quantitative analysis into consideration, more new bone formation could be estimated in the femoral and tibial bone tunnels of experimental group than that in control group.

3.3.3. Analysis of biomechanical testing

The biomechanical properties of native and reconstructive ACL from control and experimental groups were tested, together with distal femoral end and proximal tibial end. It should be noticed that the loading direction in mechanical test was different from that in native joint, but the mechanical analysis of the harvested tissue was meaningful to compare among the groups and further evaluate the functionality of HAp/Col I paste in bone tunnel healing *in vivo* (Fig. 6A, B, C). The pullout load of experimental and control groups at 12 weeks postoperatively was in the range of 130–137 N, which had no significant difference between these groups and was around one-third of the native sample's result. At 24 and 48 weeks postoperatively, the loads in experimental group increased to 155.65 ± 45.35 N and 172.54 ± 8.77 N respectively, which were significantly higher than those of the control group at 86.00 ± 21.30 N and 108.08 ± 21.52 N (Fig. 6D). Meanwhile, the maximal load of experimental group samples increased to approximately half of native ACL's maximal load (313.80 ± 47.36 N) at 24 weeks and further achieved 54.2% at 48 weeks.

To measure the cross-sectional areas of implant at breaking site, the individual autograft was wrapped with a suture thread to get its circumference and converted to diameter. Then, the tensile strength (TS) was further obtained to have a better evaluation on biomechanical property. The TS was calculated as maximum failure load divided by cross-sectional area of the autograft and the data were shown as Fig. 6E. The results illustrated that HAP/Col I paste could significantly enhance the TS of reconstructive ACL than the control samples at all time points. The TS of experimental group samples at 24 and 48 weeks achieved 9.07 ± 0.20 MPa and 11.89 ± 1.14 MPa which were 37.9–52.45% of native ACL at the same time point. In addition, all samples were broken within the intra-articular zone but not pulled out from the bone during biomechanical test, although the exact rupture sites were inconsistent. Specifically, most of the native ACL samples were broken at the tibial insertion (3 of 4 at 12 weeks, 4 of 4 at 24 weeks and 4 of 4 at 48 weeks), while the reconstructive ACL were mainly broken at the intermediate section, namely 2 of 3 at 12 weeks, 3 of 3 at 24 weeks, 4 of 4 at 48 weeks in control group, and 4 of 4 at 12 weeks, 4 of 4 at 24 weeks, 3 of 4 at 48 weeks in experimental group. It was also noticeable that 1 of 4 autografts was absorbed in the articular cavity at 12 weeks and 24 weeks respectively in control group (Table 2).

3.3.4. Histological examination

H.E. staining and Masson trichrome staining were used to validate

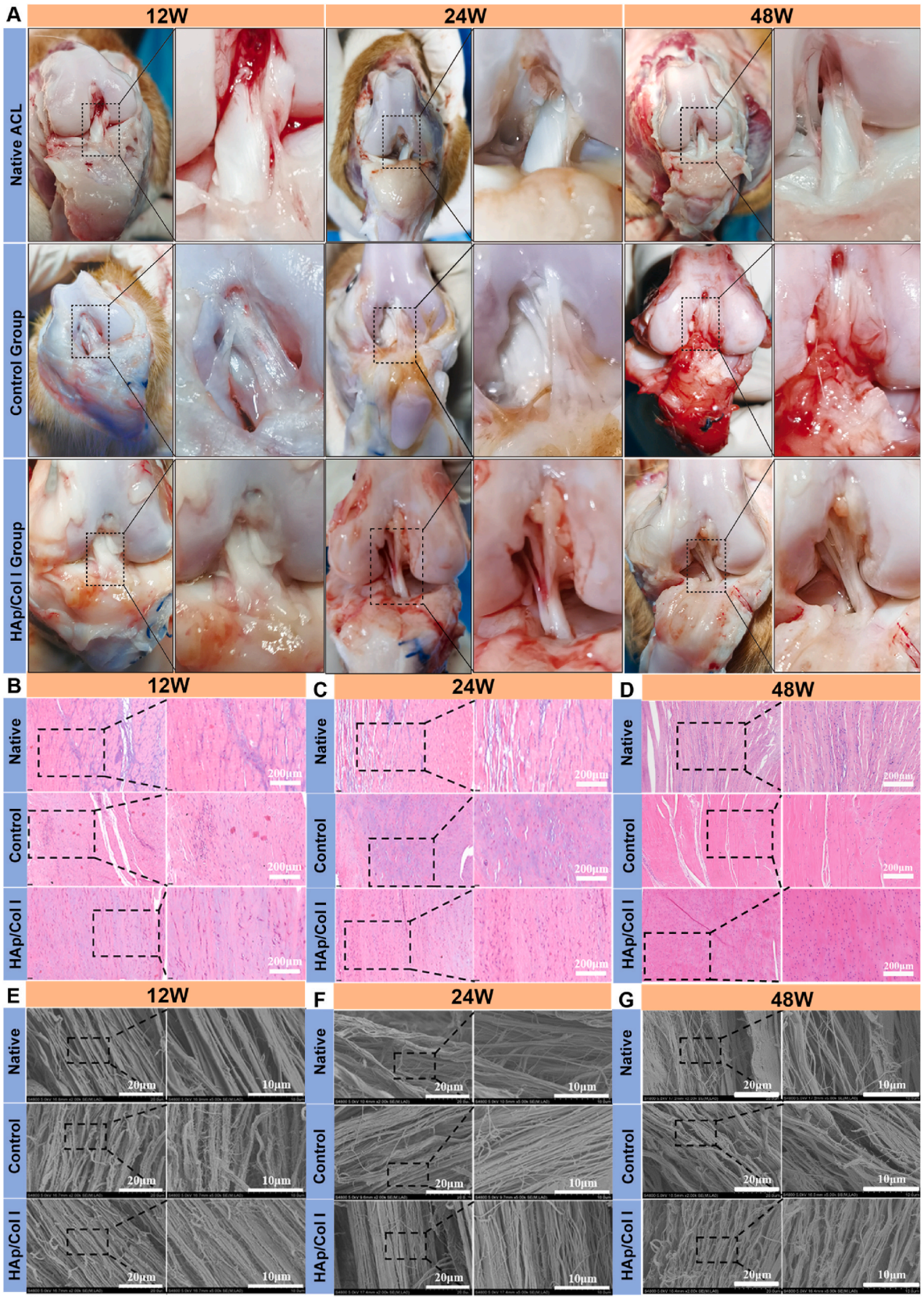

Fig. 4. The macroscopic examination, histological and morphological observation of native and reconstructive ACL. (A) The macroscopic view of native ACL, reconstructive ACL in control and experimental groups at 12, 24 and 48 weeks postoperatively. (B, C, D) Histological observation of native and reconstructive ACL at 12, 24 and 48 weeks postoperatively (H.E. left: × 200, right: × 400). (E, F, G) Morphology of native and reconstructive ACL examined by SEM at 12, 24 and 48 weeks postoperatively.

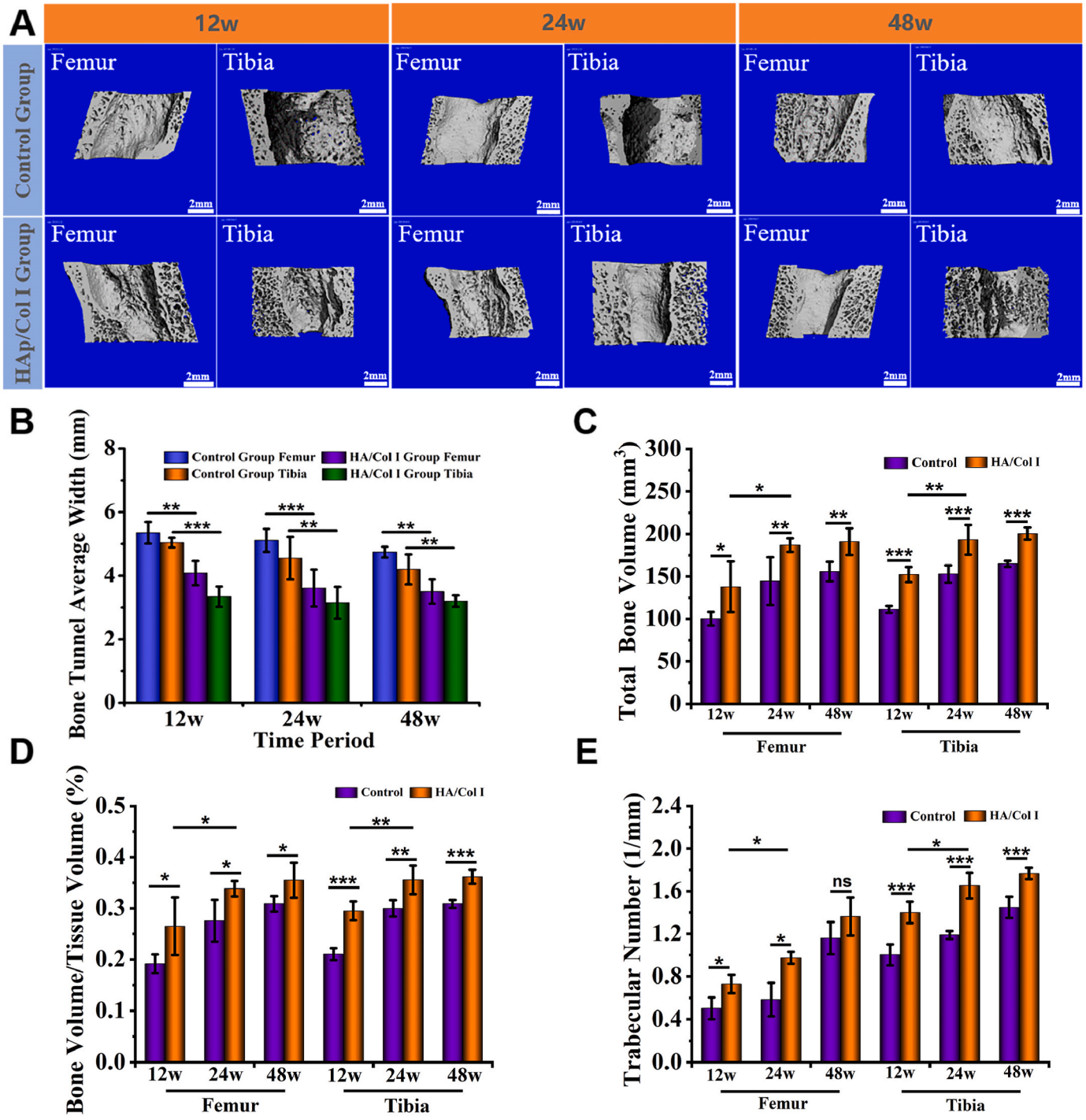

Fig. 5. Micro-CT analysis of bone tunnels in experimental and control groups. (A) Three-dimensional reconstruction images of femoral and tibial tunnels (B) The average width of tibial and femoral tunnels (n = 3). (C, D, E) Quantitative analysis results of the total bone volume (TBV), bone volume/tissue volume (BV/TV) and trabecular number (TbN) (n = 3).

the tissue formation in the tendon-bone interface, and the results were given in Fig. 7. Since the tendon-bone interface was focused in the bone tunnel in reconstructive groups, and the histological characteristic of native enthesis was well studied and reported [15,45,46], the histological results of native group were not included in this study. The histological results suggested that the tendon-bone interface treated with HAp/Col I paste was fully bridged by a new forming multi-layer structure tissue from 12 weeks to 48 weeks.

At 12 weeks, in the experimental group, the tendon-bone interface was filled with newly formed bone (green arrow) and regular collagen fibers (yellow arrow) which could be considered as Sharpey fibers since they perforated and were approximately perpendicular to the bone interface in the proximal part of the tunnel (Fig. 7D, J). In comparison, in the control group, small gaps between tendon and bone and loose connective tissue could be found (black arrow), as well as Sharpey fibers with sparser structure than those in experimental group (Fig. 7A, G). With the extension of implantation time, the morphology of newly formed tissue was improved and the cells proliferated appropriately in the experimental group.

At 24 weeks, in the experimental group, abundant Sharpey fibers

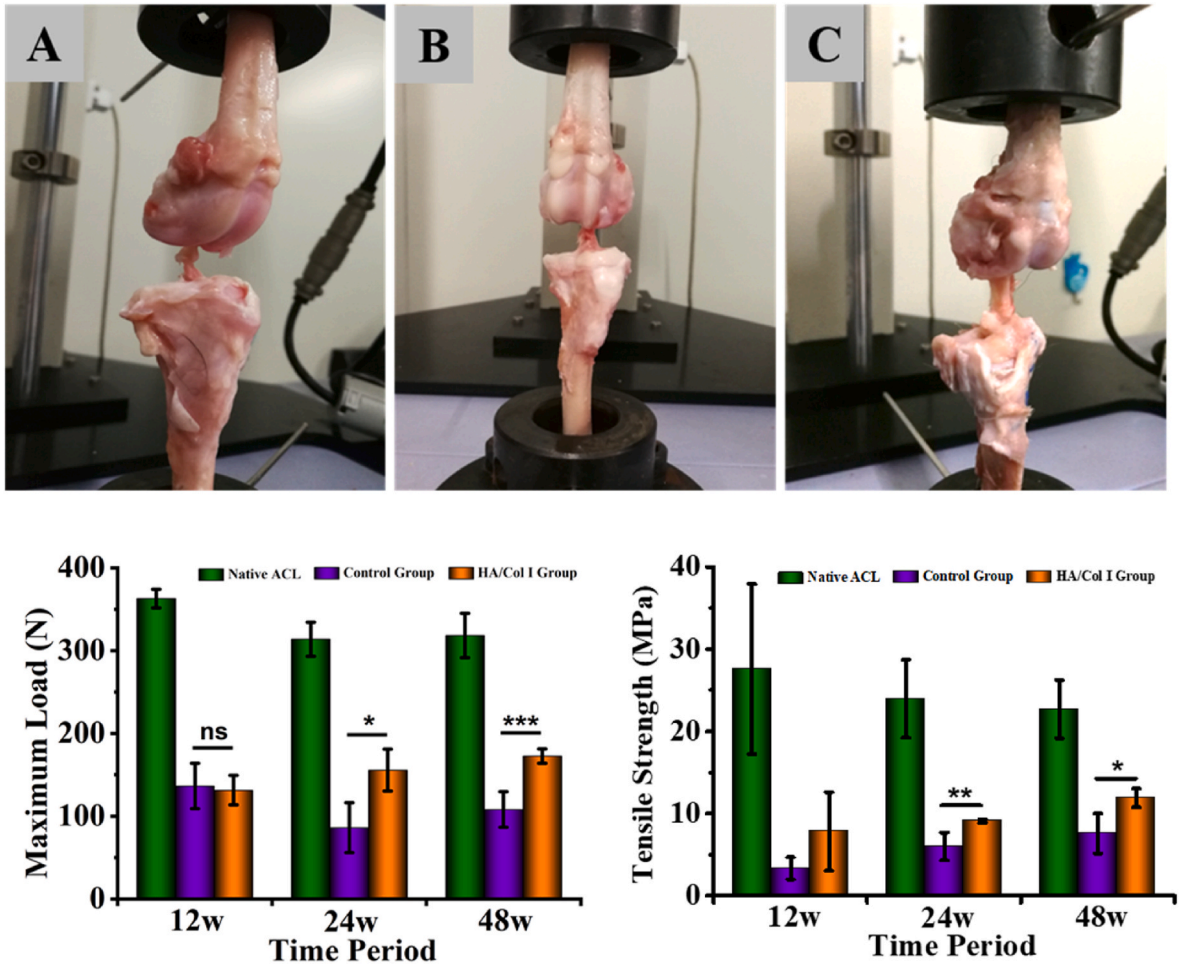

Fig. 6. The biomechanical test of native and reconstructive ACL. (A, B, C) The appearance of biomechanical test samples from native, control and experimental groups, respectively. (D, E) The maximum load and tensile strength of test samples from native, control and experimental groups, respectively (n = 4). The statistical analysis manifested the test number was enough to achieve statistical power (90%).

Table 2
The failure point statistics on the graft complex.

Time	Group (n = 4)	Graft midsubstance	ACL femoral origin	ACL tibial insertion	Femoral or tibial pullout	Graft absorption
12 weeks	Native ACL	1	0	3	0	0
	Control Group	2	0	1	0	1
	HAp/Col I Group	4	0	0	0	0
24 weeks	Native ACL	0	0	4	0	0
	Control Group	3	0	0	0	1
	HAp/Col I Group	4	0	0	0	0
48 weeks	Native ACL	0	0	4	0	0
	Control Group	4	0	0	0	0
	HAp/Col I Group	3	0	1	0	0

could be found anchored directly onto the newly formed bone leading to an indistinct boundary. Meanwhile, a portion of the tendon-bone interface replicated the fibrocartilaginous transition zone which existed in native tissue [47], but the calcified fibrocartilage and tide line were not observed (Fig. 7E, K). In the control group, tense Sharpey fibers could be found at the tendon-bone interface, no chondrocytes or cartilage-like tissues were found here (Fig. 7B, H).

At 48 weeks, the histological staining images gave clues that well-defined four-layer structure of insertion site could be regenerated in the experimental group, including tendon tissue, fibrocartilage, calcified fibrocartilage and bone. A regular marking of the tide line between fibrous cartilage and calcified cartilage could also be observed (Fig. 7F, L). In the control group, more and compact Sharpey fibers linked directly from tendon to bone, with a clear boundary and morphology similar to those in the experimental group at 12 weeks, while no fibrocartilage and calcified cartilage were observed (Fig. C, I).

4. Discussion

As one of the connections between femur and tibia, ACL and its terminal structure plays an important role in physiological and biological functions of knee joint. The gradient composition and structure can not only transmit and balance stress, but also regulate the growth and collagen remodeling of tendon or ligament. As a result, the restoration of gradient composition and structure in reconstructive ACL is crucial to its physiological function recovery and normal daily life of patients. The

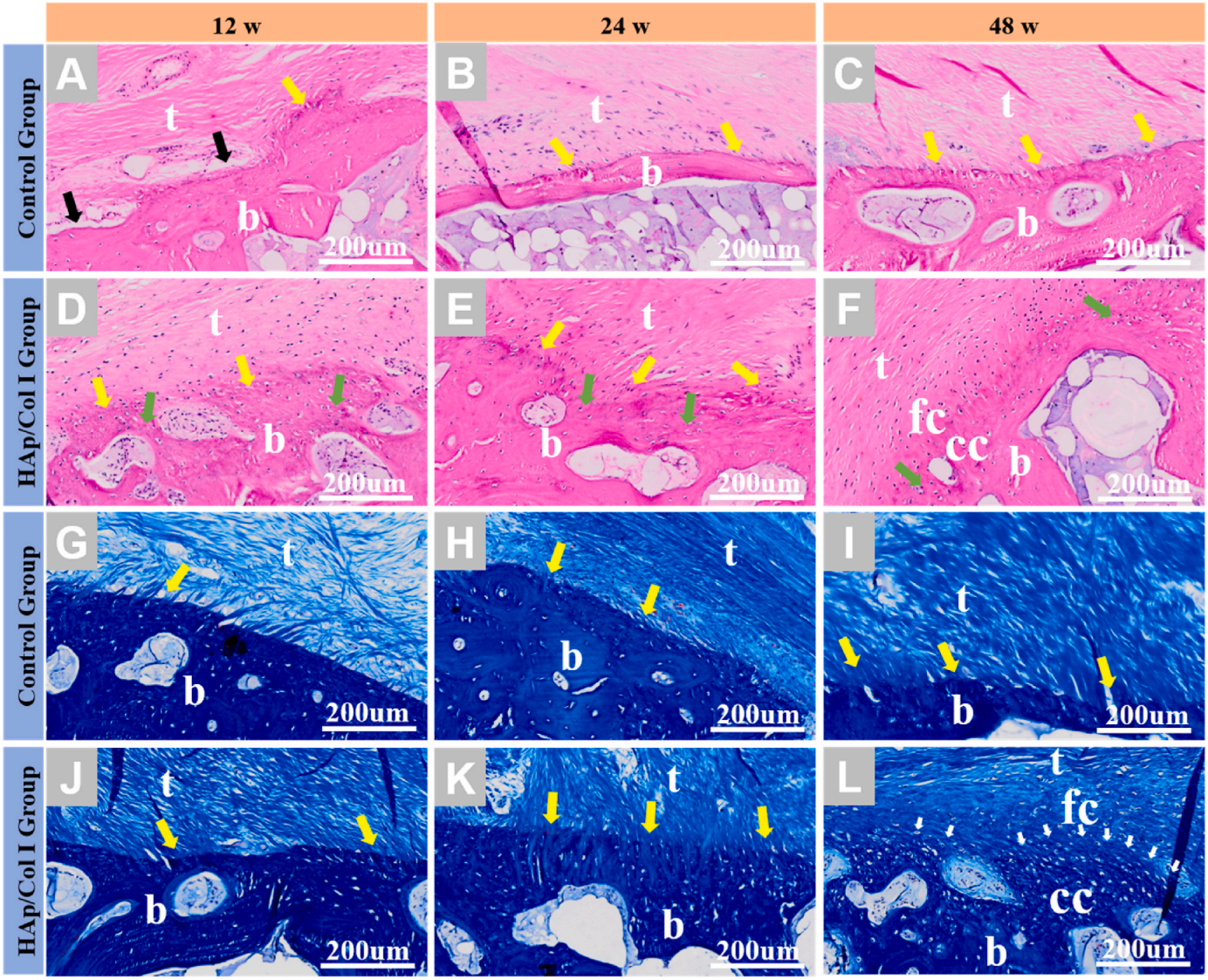

Fig. 7. Histological observation of healed bone tunnels in experimental and control groups. (A–F) H.E. staining (× 200). (G–L) Masson trichrome staining (× 200). (t: tendon; fc: fibrocartilage; cc: calcified cartilage; b: bone; black arrow: small gaps between tendon and bone; yellow arrow: Sharpey-like fibers; green arrow: newly formed bone; white arrow: tide markers).

ACL insertion site which is the part of the tendon in bone tunnel could be the weak link in the early stage of ACL reconstruction. Therefore, an accelerated and enhanced early healing of tendon-bone could be beneficial to the successful ACL reconstruction.

It is well established that bone tunnel is healed with an intervening layer of fibrovascular scar tissue between the graft and bone [13,48]. Previous studies on ACL reconstruction using biological graft drew a consistent conclusion that graft would undergo a "ligamentization" process after the implantation, including stages like tissue necrosis, new tissue growth replacement, remodeling and maturation [49,50]. In the remodeling stage, the migrated and proliferated osteogenic cells at the fibrous interface secreted and generated new extracellular matrix, and the interface was gradually modeled to develop a Sharpey fiber-like local structure which could increase the connection strength [51]. However, such scar tissue was mechanically inferior to native tissue and became a "weak link" after surgical reconstruction. For these reasons, there is much interest in developing interventions that can accelerate and improve the healing of tendon-bone interface. Several approaches have been studied in this field, including the application of transforming growth factor (TGF) [52,53], bone morphogenetic protein (BMP) [54,55], gene transfection [25], stem cells [56,57], platelet rich plasma (PRP) [58], autogenous periosteum [22] and calcium-based cements [59,60].

In light of the theory of tissue inducing biomaterials and our previous research, we hypothesized that constructing an appropriate microenvironment with suitable biomaterials to regulate cell behavior probably could accelerate and enhance the tendon-bone interface healing during ACL reconstruction. Since both bone and ligament were involved during the compositional and structural restoration, calcium phosphate and collagen based biomaterial should hold great potential owing to their physicochemical and biological advantages.

Calcium phosphates including hydroxyapatite have been proven with excellent biocompatibility, osteoconductivity and osteoinductivity [61–63], were further studied to promote the bone growth in tendon-bone healing. For instance, Matsuzaki et al. [64] reported on the use of hybridized semitendinosus tendon grafts with a calcium phosphate-containing solution to perform ACL reconstructions in rabbits, and found that new bone and cartilage was formed around the tendon grafts at 3 weeks. Pan W et al. [60] evaluated the ability of injectable calcium phosphate cement (ICPC) together with xenograft and growth factor to enhance the tendon-bone healing, they noted the interface tissue contained more new bone and the space between the

grafted tendon and the bone tunnel was narrower than the control.

Even though calcium phosphates showed outstanding osteogenesis, they still need suitable carriers to transfer. Meanwhile, because the ECM of ACL was composed primarily of 90% type I collagen [65], type I collagen hydrogel was developed to combine with the inorganic calcium phosphates. Collagen hydrogels could provide microenvironment such as suitable adhesion sites, proliferate space and transfer channels for nutrition and metabolite for cell attachment, proliferation, and differentiation [66,67], including cell sources such as fibroblasts, osteoblasts and MSCs [68–70]. Moreover, collagen served as a functional bioreactor which could provide various cytokines and physiological cyclic loading to induce the differentiation and expression of cells [36]. Recently, increasing attentions were paid to use type I collagen hydrogel to repair cartilage injury, which have achieved good results [71,72]. Thus type I collagen could promote the formation of an enthesis with gradient structures during the ACL reconstruction.

In this study, an injectable paste based on hydroxyapatite and type I collagen was prepared and evaluated to accelerate and improve the tendon-bone healing in a canine ACL reconstruction model. The compositional and structural properties of the HAp/Col I paste were systematical characterized, as well as their stability and injectable performance. The optimized HAp/Col I paste was composed of spherical HAp (40 wt%) with low crystallinity and Col I solution (60 wt%), as approved by the thermal analysis shown in Fig. 1B. Both SEM and Alizarin red staining of the paste indicated the homogeneous distribution of HAps in collagen solution, which was not only beneficial to the systemic stability and easy injection, but would also provide open and inter-connecting pores after the degradation of collagen *in vivo*. Injectable calcium phosphate cement was applied to heal the tendon-bone, but the osteointegration of grafted tendon in bone tunnels was unsatisfied because of the slow degradation and compact spatial structure [60,73].

The collagen could be rapidly degraded and absorbed *in vivo* [74], which leads to the formation of an interconnected porous structure. The porous structure allows the migration and proliferation of cells as well as vascularization [75,76]. Thus, the HAp/Col I paste composed of calcium phosphate particles and degradable organic carrier could provide the necessary compositional and spatial support to the tissue regeneration in the bone tunnel. Based on 24 staining images, the area ratio of pores to the visual field was statistically calculated using Image J. Accordingly, the pore area accounted for around 39.4% ± 1.13% of the whole visual field in the images. It could be inferred that the final porosity of the implant was around 40%, which would allow cell migration, proliferation and vascularization [75].

Previous single bundle ACL reconstruction by autogenous semitendinosus tendon stated that tissue necrosis happened in the bone tunnel at 2 weeks and new tissue grew into and replaced from the edge of ligament at 4 weeks [50]. While collagen-based biomaterial was considered to be fully degraded and absorbed in 4–8 weeks [34,36], the degradation of collagen in HAp/Col I paste might be synchronous or slightly delayed with the tissue necrosis and new tissue growth stages in the bone tunnel. Meanwhile, the pores produced by the continuous degradation of collagen would be replaced by the growth of new tissue, forming a dynamic repair process to improve the interface integration between tendon and bone.

Because collagen could be self-assembled at the body temperature [77], the HAp/Col I paste could be gelled and stabilized when it was injected into aqueous phase as shown in Fig. 2H. The stability ensured that the paste could be directly operated and injected into the bone tunnel under arthroscopy [78]. And the detection of Ca and P contents under the given extraction condition implied the gelation of collagen could stabilize the paste and majority of the implant could be maintained in the bone tunnel after the implantation.

Because the HAp/Col I paste was prepared by physically mixing two materials with excellent biocompatibility under controlled conditions, the *in vitro* study verified the paste was cell compatible and the MC3T3-E1 cells could appropriately proliferate and osteogenically express when HAp was encapsulated in the paste. Further investigation may also need to elucidate the mechanism of the material-cell interaction in the future with evaluation methods including western blotting, immunofluorescence, and proteomics.

After the *in vivo* implantation and harvest of the pastes at different time points, the results of general observation, micro-CT analysis, biomechanical test and histological examination indicated that the HAp/Col I paste could accelerate and enhance the tendon-bone interface healing in the bone tunnel of ACL reconstruction. According to the 3D reconstruction of micro-CT scan shown in Fig. 5A, an enlarged opening of the bone tunnel near the articular cavity was observed, which was especially obvious in the control group. The average bone tunnel width was significantly bigger than that in experimental groups, both in femur and tibia as statistics shown in Fig. 5B. The enlarged bone tunnel was not only related to the windshield wiper effect caused by animal activity, but also to the effects of proteolytic enzymes, cytokines and growth factor inhibitors in the synovial fluid. It has been reported that proteolytic enzymes in synovial fluid can inhibit bone growth, delay tendon healing and enlarge bone tunnel [79,80]. Particularly, according to the results displayed in Fig. 5C and D, graft resorption was found at 12 and 24 weeks respectively in the control group, which may be the result of increased collagenase activity owing to the change of biological factors in synovial fluid. In the experimental group, the collagen gel formed onsite *in vivo* could form a barrier at the entrance of the bone tunnel to prevent the graft from being over-exposed to the synovial fluid. Meanwhile, the as-filled paste was beneficial to improve the interface between tendon and bone tunnel, which was drilled manually with matching design, but the gaps between graft and bone tunnel were inevitable. The increased contact and compaction between graft and bone tunnel further reduced the abrasion of the graft and increased the compressive stress on graft which was in favor of cartilage formation [40,81,82]. On the other hand, the increase of BV, BV/TV and TbN as shown in Fig. 5C, D and 5E indicated the generation of new bone tissue owing to the implanted HAp/Col I paste in the experim.ental group. These factors combined together may lead to different tightness of collagen bundle in reconstructive ACL and contractility at the opening of bone tunnel.

As shown in the histological examination, a typical four-layer transitional structure at the interface between tendon and bone was found in the experimental group at 24 weeks. The graft implanted without the paste was healed with a structure containing ligament, Sharpey fibers and bone [51], as found in control group. The highly differentiated structures were analogous to the native anatomy and could definitely disperse the stress on the ligament [18] and therefore improve the biomechanical property in the experimental group. It could be inferred that the filling of paste in the bone tunnel not only increased the physical contact between the graft and bone tunnel, but also changed the microenvironment compositionally and structurally which influenced the reconstructive interface. The collagen component in the paste could provide the scaffold for cell migration, attachment and proliferation shortly after the implantation. The gradual degradation of collagen provided the consumable raw materials for cells and further made room for the newly-formed extracellular matrix, which was a dynamic process and played an important role in remodeling of the transitional structure at the interface between tendon and bone. At the longer term after the implantation, the HAp component in the paste could regulate the osteogenic expression and induce the new bone formation [32]. The intertwining interactions among the graft components, cells and host bone tissues led to a better healing of the tendon-bone interface.

The biomechanical property of graft was so important that it would affect the graft itself and the reconstructed ACL, it would also influence the remodeling structure between graft and bone tunnel. It was reported that the graft's mechanical properties and physical signals could direct cellular activity and phenotype toward functional tissue assembly and mechanical competent tissue repair [83]. Frank et al. [84] pointed out that the biomechanical strength of the autologous graft would firstly decrease after auto-transplantation, then gradually increase and finally

could restore only 10%–50% of the native tissue's strength.

In this study, the reconstructive ACL with enhanced healing of tendon-bone interface could achieve around half of maximal load of native tissue at 24 weeks. Therefore, the reconstructive ACL could provide enough strength at early stage since the ACL was loaded only about 20% of its failure load during daily activities [85]. Among the many factors could affect the shaping of tendon fibers, the enhanced tendon-to-bone interface could fix the graft ends and then mechanical stimulation could be correctly loaded on the graft which had positive influence on the tendon fiber remodeling. The shortened shaping period and matured tendon fibers could be beneficial to increase the mechanical property of the reconstructed ligament. Comparing the mechanical results between control and experimental groups, the earlier and intenser interaction between graft and bone tissue could be considered as one of the major reasons. As displayed in histological staining, Sharpey fibers could be observed anchored directly onto the newly formed bone without obvious gap in experimental group as early as 12 weeks, and the connection was so intense and universal at the interface that the boundary was blur at 24 weeks. The abundant and dense Sharpey fibers contributed significantly to the biomechanical properties of reconstructive tissue. The matured tendon-to-bone interface structure could enhance the mechanical property theoretically, however, the mechanical test results were not significantly improved after 24 weeks. The major reason was that the testing force was loaded on the entire graft complex but not focused on the tendon-to-bone interface, leading to reflect the lowest mechanical strength in the reconstructive ACL. Therefore, the current extensively applied biomechanical test method should be further modified to meet the requirements for mechanical test of tendon-to-bone interface.

5. Conclusion

In summary, the results of this study suggested that an injectable HAp/Col I paste could improve tendon-bone healing in a canine ACL reconstruction with autogenous tendon as evidenced by medical imaging, biomechanical and histologic results. A compositional and structural gradient, especially a typical four-layer transitional structure could be restored at the interface between tendon and bone, which was similar to the anatomical structure of normal ACL. The potential of using this injectable hydroxyapatite/collagen type I paste to promote tendon-bone healing and reduce the risk of reconstruction failure would be attractive for ligament or tendon regeneration, and further provide a practicable solution for clinical issues.

Ethics approval and consent to participate

The animal study was approved by the Ethical Committee of Sichuan University (No. K2017055). All the animals were purchased from Beagle Breeding and Experimental Service Platform of Sichuan Institute of Musk Deer Breeding, and the animal certification is No. SCXK (Chuan) 2015–01. The animal experiment guidance from the ethical committee and the guide for care and use of laboratory animals from NIH were followed during the whole experiment course.

CRediT authorship contribution statement

Qingsong Jiang: Validation, Formal analysis, Investigation, Writing – original draft, Visualization. **Liren Wang:** Validation, Investigation, Writing – original draft. **Zhanhong Liu:** Investigation, Formal analysis, Writing – review & editing, Visualization. **Jinlei Su:** Investigation. **Yajun Tang:** Investigation. **Peijie Tan:** Investigation. **Xiangdong Zhu:** Methodology, Funding acquisition. **Kai Zhang:** Methodology. **Xing Ma:** Methodology. **Jia Jiang:** Methodology, Validation, Resources, Project administration. **Jinzhong Zhao:** Conceptualization, Methodology, Supervision, Funding acquisition. **Hai Lin:** Conceptualization, Methodology, Validation, Investigation, Resources, Writing – review & editing, Supervision, Project administration, Funding acquisition. **Xingdong Zhang:** Conceptualization, Supervision.

Declaration of competing interest

The authors declare no competing financial interests in this work.

Acknowledgement

This work was financially supported by the National Key Research and Development Program of China (2018YFC1106200 and 2018YFC1106203), the National Natural Science Foundation of China (32071330), the Sichuan Science and Technology Innovation Team (2019JDTD0008) and the Key Science and Technology Program of Guangxi Province (AA17204085-2). The graphic abstract was created with BioRender.com.

Appendix A. Supplementary data

Supplementary data to this article can be found online at https://doi.org/10.1016/j.bioactmat.2022.05.003.

References

[1] C.D. Harner, J.R. Giffin, R.C. Dunteman, C.C. Annunziata, M.J. Friedman, Evaluation and treatment of recurrent instability after anterior cruciate ligament reconstruction, Instr. Course Lect. 50 (2001) 463–474.
[2] B. Moses, J. Orchard, J. Orchard, Systematic review: annual incidence of acl injury and surgery in various populations, Res. Sports Med. 20 (3–4) (2012) 157–179.
[3] A. von Porat, E.M. Roos, H. Roos, High prevalence of osteoarthritis 14 years after an anterior cruciate ligament tear in male soccer players: a study of radiographic and patient relevant outcomes, Ann. Rheum. Dis. 63 (3) (2004) 269–273.
[4] D.J. Biau, S. Katsahian, J. Kartus, A. Harilainen, J.A. Feller, M. Sajovic, L. Ejerhed, S. Zaffagnini, M. Roepke, R. Nizard, Patellar tendon versus hamstring tendon autografts for reconstructing the anterior cruciate ligament a meta-analysis based on individual patient data, Am. J. Sports Med. 37 (12) (2009) 2470–2478.
[5] D.E. Cooper, X.H.H. Deng, A.L. Burstein, R.F. Warren, The strength of the central 3rd patellar tendon graft - a biomechanical study, Am. J. Sports Med. 21 (6) (1993) 818–824.
[6] D.C. Taylor, T.M. DeBerardino, B.J. Nelson, M. Duffey, J. Tenuta, P.D. Stoneman, R.X. Sturdivant, S. Mountcastle, Patellar tendon versus hamstring tendon autografts for anterior cruciate ligament reconstruction a randomized controlled trial using similar femoral and tibial fixation methods, Am. J. Sports Med. 37 (10) (2009) 1946–1957.
[7] P.K. Gupta, A. Acharya, A. Mourya, P. Mahajan, Comparison of patellar tendon versus hamstrings autografts for anterior cruciate ligament reconstruction in indian population: a randomised control trial study, J. Clin. Orthopaed. Trauma 10 (3) (2019) 581–585.
[8] K. Stanczak, M. Zielinska, M. Synder, M. Domzalski, M. Polguj, M. Sibinski, Comparison of hamstring and patellar tendon grafts in anterior cruciate ligament reconstruction: a prospective randomized study, J. Int. Med. Res. 46 (2) (2018) 785–791.
[9] J.J. Bonamo, R.M. Krinick, A.A. Sporn, Rupture of the patellar ligament after use of its central 3rd for anterior cruciate reconstruction - a report of 2 cases, J. Bone Joint Surg. Am. 66A (8) (1984) 1294–1297.
[10] B. Christen, R.P. Jakob, Fractures associated with patellar ligament grafts in cruciate ligament surgery, J. Bone Joint Surg. British 74 (4) (1992) 617–619.
[11] V.K. Goradia, M.C. Rochat, W.A. Grana, M.D. Rohrer, H.S. Prasad, Tendon-to-bone healing of a semitendinosus tendon autograft used for acl reconstruction in a sheep model, Am. J. Knee Surg. 13 (3) (2000) 143–151.
[12] S.A. Rodeo, S.P. Arnoczky, P.A. Torzilli, C. Hidaka, R.F. Warren, Tendon-healing in a bone tunnel - a biomechanical and histological study in the dog, J. Bone Joint Surg. Am. 75A (12) (1993) 1795–1803.
[13] B.R. Freedman, G.W. Fryhofer, N.S. Salka, H.A. Raja, C.D. Hillin, C.A. Nuss, D. C. Farber, L.J. Soslowsky, Mechanical, histological, and functional properties remain inferior in conservatively treated achilles tendons in rodents: long term evaluation, J. Biomech. 56 (2017) 55–60.
[14] L.M. Galatz, L.J. Sandell, S.Y. Rothermich, R. Das, A. Mastny, N. Havlioglu, M. J. Silva, S. Thomopoulos, Characteristics of the rat supraspinatus tendon during tendon-to-bone healing after acute injury, J. Orthop. Res. 24 (3) (2006) 541–550.
[15] H.H. Lu, S. Thomopoulos, Functional attachment of soft tissues to bone: Development, healing, and tissue engineering, in: M.L. Yarmush (Ed.), Annual Review of Biomedical Engineering, 15 2013, pp. 201–226.
[16] H.M. Shaw, M. Benjamin, Structure-function relationships of entheses in relation to mechanical load and exercise, Scand. J. Med. Sci. Sports 17 (4) (2007) 303–315.
[17] L. Smith, Y. Xia, L.M. Galatz, G.M. Genin, S. Thomopoulos, Tissue-engineering strategies for the tendon/ligament-to-bone insertion, Connect. Tissue Res. 53 (2) (2012) 95–105.

[18] A.C. Deymier-Black, J.D. Pasteris, G.M. Genin, S. Thomopoulos, Allometry of the tendon enthesis: mechanisms of load transfer between tendon and bone, J. Biomech. Eng. Transact. Asme 137 (11) (2015).

[19] A.G. Schwartz, J.D. Pasteris, G.M. Genin, T.L. Daulton, S. Thomopoulos, Mineral distributions at the developing tendon enthesis, PLoS One 7 (11) (2012).

[20] B. Wopenka, A. Kent, J.D. Pasteris, Y. Yoon, S. Thomopoulos, The tendon-to-bone transition of the rotator cuff: a preliminary Raman spectroscopic study documenting the gradual mineralization across the insertion in rat tissue samples, Appl. Spectrosc. 62 (12) (2008) 1285–1294.

[21] X. Han, L. Guo, F. Wang, Q. Zhu, L. Yang, Contribution of pthrp to mechanical strain-induced fibrochondrogenic differentiation in entheses of achilles tendon of miniature pigs, J. Biomech. 47 (10) (2014) 2406–2414.

[22] I. Youn, D.G. Jones, P.J. Andrews, M.P. Cook, J.K.F. Suh, Periosteal augmentation of a tendon graft improves tendon healing in the bone tunnel, Clin. Orthop. Relat. Res. 419 (2004) 223–231.

[23] S. Font Tellado, E.R. Balmayor, M. Van Griensven, Strategies to engineer tendon/ligament-to-bone interface: biomaterials, cells and growth factors, Adv. Drug Deliv. Rev. 94 (2015) 126–140.

[24] H. Fan, H. Liu, S.L. Toh, J.C.H. Goh, Anterior cruciate ligament regeneration using mesenchymal stem cells and silk scaffold in large animal model, Biomaterials 30 (28) (2009) 4967–4977.

[25] C. Lattermann, B.A. Zelle, J.D. Whalen, A.W.A. Baltzer, P.D. Robbins, C. Niyibizi, C.H. Evans, F.H. Fu, Gene transfer to the tendon-bone insertion site, Knee Surg. Sports Traumatol. Arthrosc. 12 (5) (2004) 510–515.

[26] P. Weimin, L. Dan, W. Yiyong, H. Yunyu, Z. Li, Tendon-to-bone healing using an injectable calcium phosphate cement combined with bone xenograft/bmp composite, Biomaterials 34 (38) (2013) 9926–9936.

[27] S. Patel, J.-M. Caldwell, S.B. Doty, W.N. Levine, S. Rodeo, L.J. Soslowsky, S. Thomopoulos, H.H. Lu, Integrating soft and hard tissues via interface tissue engineering, J. Orthop. Res. 36 (4) (2018) 1069–1077.

[28] S. Kawamura, L. Ying, H.J. Kim, C. Dynybil, S.A. Rodeo, Macrophages accumulate in the early phase of tendon-bone healing, J. Orthop. Res. 23 (6) (2005) 1425–1432.

[29] P. Sharma, N. Maffulli, Current concepts review tendon injury and tendinopathy: healing and repair, J. Bone Joint Surg. Am. 87A (1) (2005) 187–202.

[30] J.V. Loghem, Y.A. Yutskovskaya, W. Philip Werschler, Calcium hydroxylapatite: over a decade of clinical experience, J. Clin. Aesth. Dermatol. 8 (1) (2015) 38–49.

[31] N. Rajan, J. Habermehl, M.-F. Cote, C.J. Doillon, D. Mantovani, Preparation of ready-to-use, storable and reconstituted type i collagen from rat tail tendon for tissue engineering applications, Nat. Protoc. 1 (6) (2006) 2753–2758.

[32] P. He, S. Sahoo, K.S. Ng, K. Chen, S.L. Toh, J.C.H. Goh, Enhanced osteoinductivity and osteoconductivity through hydroxyapatite coating of silk-based tissue-engineered ligament scaffold, J. Biomed. Mater. Res. 101 (2) (2013) 555–566.

[33] S. Hesaraki, H. Nazarian, M. Pourbaghi-Masouleh, S. Borhan, Comparative study of mesenchymal stem cells osteogenic differentiation on low-temperature biomineralized nanocrystalline carbonated hydroxyapatite and sintered hydroxyapatite, J. Biomed. Mater. Res. B Appl. Biomater. 102 (1) (2014) 108–118.

[34] N. Daei-farshbaf, A. Ardeshirylajimi, E. Seyedjafari, A. Piryaei, F.F. Fathabady, M. Hedayati, M. Salehi, M. Soleimani, H. Nazarian, S.-L. Moradi, M. Norouzian, Bioceramic-collagen scaffolds loaded with human adipose-tissue derived stem cells for bone tissue engineering, Mol. Biol. Rep. 41 (2) (2014) 741–749.

[35] R.J. Kane, H.E. Weiss-Bilka, M.J. Meagher, Y. Liu, J.A. Gargac, G.L. Niebur, D. R. Wagner, R.K. Roeder, Hydroxyapatite reinforced collagen scaffolds with improved architecture and mechanical properties, Acta Biomater. 17 (2015) 16–25.

[36] T. Long, J. Yang, S.-S. Shi, Y.-P. Guo, Q.-F. Ke, Z.-A. Zhu, Fabrication of three-dimensional porous scaffold based on collagen fiber and bioglass for bone tissue engineering, J. Biomed. Mater. Res. B Appl. Biomater. 103 (7) (2015) 1455–1464.

[37] E. Quinlan, A. Lopez-Noriega, E. Thompson, H.M. Kelly, S.A. Cryan, F.J. O'Brien, Development of collagen-hydroxyapatite scaffolds incorporating plga and alginate microparticles for the controlled delivery of rhbmp-2 for bone tissue engineering, J. Contr. Release 198 (2015) 71–79.

[38] R.D. Sumanasinghe, S.H. Bernacki, E.G. Loboa, Osteogenic differentiation of human mesenchymal stem cells in collagen matrices: effect of uniaxial cyclic tensile strain on bone morphogenetic protein (bmp-2) mrna expression, Tissue Eng. 12 (12) (2006) 3459–3465.

[39] Title, - din en iso 10993-12:2012-10.

[40] M. Benjamin, J.R. Ralphs, Fibrocartilage in tendons and ligaments - an adaptation to compressive load, J. Anat. 193 (1998) 481–494.

[41] V.K. Goradia, M.C. Rochat, M. Kida, W.A. Grana, Natural history of a hamstring tendon autograft used for anterior cruciate ligament reconstruction in a sheep model, Am. J. Sports Med. 28 (1) (2000) 40–46.

[42] P.E. Scranton, W.L. Lanzer, M.S. Ferguson, T.R. Kirkman, D.S. Pflaster, Mechanisms of anterior cruciate ligament neovascularization and ligamentization, Arthroscopy 14 (7) (1998) 702–716.

[43] R.P.A. Janssen, S.U. Scheffler, Intra-articular remodelling of hamstring tendon grafts after anterior cruciate ligament reconstruction, Knee Surg. Sports Traumatol. Arthrosc. 22 (9) (2014) 2102–2108.

[44] M. Sanchez, E. Anitua, J. Azofra, R. Prado, F. Muruzabal, I. Andia, Ligamentization of tendon grafts treated with an endogenous preparation rich in growth factors: gross morphology and histology, Arthroscop. J. Arthroscop. Relat. Surg. 26 (4) (2010) 470–480.

[45] S. Font Tellado, E.R. Balmayor, M. Van Griensven, Strategies to engineer tendon/ligament-to-bone interface: biomaterials, cells and growth factors, Adv. Drug Deliv. Rev. 94 (2015) 126–140.

[46] R. Newsham-West, H. Nicholson, M. Walton, P. Milburn, Long-term morphology of a healing bone–tendon interface: a histological observation in the sheep model, J. Anat. 210 (3) (2007) 318–327.

[47] J.K. Lee, S. Lee, C.S. Sang, M.C.J.K.S. Lee, Arthroscopy Sports Traumatology, Anatomy of the Anterior Cruciate Ligament Insertion Sites: Comparison of Plain Radiography and Three-Dimensional Computed Tomographic Imaging to Anatomic Dissection, 2015.

[48] D. Lin, P. Alberton, M.D. Caceres, E. Volkmer, M. Schieker, D. Docheva, Tenomodulin is essential for prevention of adipocyte accumulation and fibrovascular scar formation during early tendon healing, Cell Death Dis. 8 (2017).

[49] S. Claes, P. Verdonk, R. Forsyth, J. Bellemans, The "ligamentization" process in anterior cruciate ligament reconstruction what happens to the human graft? A systematic review of the literature, Am. J. Sports Med. 39 (11) (2011) 2476–2483.

[50] K. Marumo, M. Saito, T. Yamagishi, K. Fujii, The "ligamentization" process in human anterior cruciate ligament reconstruction with autogenous patellar and hamstring tendons - a biochemical study, Am. J. Sports Med. 33 (8) (2005) 1166–1173.

[51] A. Weiler, R.F.G. Hoffmann, H.J. Bail, O. Rehm, N.P. Sudkamp, Tendon healing in a bone tunnel. Part ii: histologic analysis after biodegradable interference fit fixation in a model of anterior cruciate ligament reconstruction in sheep, Arthroscop. J. Arthroscop. Relat. Surg. 18 (2) (2002) 124–135.

[52] H.M. Kim, L.M. Galatz, R. Das, N. Havlioglu, S.Y. Rothermich, S. Thomopoulos, The role of transforming growth factor beta isoforms in tendon-to-bone healing, Connect. Tissue Res. 52 (2) (2011) 87–98.

[53] K. Yasuda, F. Tomita, S. Yamazaki, A. Minami, H. Tohyama, The effect of growth factors on biomechanical properties of the bone-patellar tendon-bone graft after anterior cruciate ligament reconstruction - a canine model study, Am. J. Sports Med. 32 (4) (2004) 870–880.

[54] Y. Dong, Q. Zhang, Y. Li, J. Jiang, S. Chen, Enhancement of tendon-bone healing for anterior cruciate ligament (acl) reconstruction using bone marrow-derived mesenchymal stem cells infected with bmp-2, Int. J. Mol. Sci. 13 (10) (2012) 13605–13620.

[55] C.B. Ma, S. Kawamura, X.-H. Deng, L. Ying, J. Schneidkraut, P. Hays, S.A. Rodeo, Bone morphogenetic proteins-signaling plays a role in tendon-to-bone healing - a study of rhbmp-2 and noggin, Am. J. Sports Med. 35 (4) (2007) 597–604.

[56] H. Obaid, D. Connell, Cell therapy in tendon disorders what is the current evidence? Am. J. Sports Med. 38 (10) (2010) 2123–2132.

[57] H.W. Ouyang, J.C.H. Goh, E.H. Lee, Use of bone marrow stromal cells for tendon graft-to-bone healing - histological and immunohistochemical studies in a rabbit model, Am. J. Sports Med. 32 (2) (2004) 321–327.

[58] M. Wadhwa, M.J. Seghatchian, A. Lubenko, M. Contreras, P. Dilger, C. Bird, R. Thorpe, Cytokine levels in platelet concentrates: quantitation by bioassays and immunoassays, Br. J. Haematol. 93 (1) (1996) 225–234.

[59] L.V. Gulotta, D. Kovacevic, L. Ying, J.R. Ehteshami, S. Montgomery, S.A. Rodeo, Augmentation of tendon-to-bone healing with a magnesium-based bone adhesive, Am. J. Sports Med. 36 (7) (2008) 1290–1297.

[60] W. Pan, D. Li, Y. Wei, Y. Hu, L. Zhou, Tendon-to-bone healing using an injectable calcium phosphate cement combined with bone xenograft/bmp composite, Biomaterials 34 (38) (2013) 9926–9936.

[61] J.P. Gleeson, N.A. Plunkett, F.J. O'Brien, Addition of hydroxyapatite improves stiffness, interconnectivity and osteogenic potential of a highly porous collagen-based scaffold for bone tissue regeneration, Eur. Cell. Mater. 20 (2010) 218–230.

[62] X. Huang, S. Bai, Q. Lu, X. Liu, S. Liu, H. Zhu, Osteoinductive-nanoscaled silk/ha composite scaffolds for bone tissue engineering application, J. Biomed. Mater. Res. B Appl. Biomater. 103 (7) (2015) 1402–1414.

[63] L.R. Liu, L.H. Zhang, B.Z. Ren, F.J. Wang, Q.Q. Zhang, Preparation and characterization of collagen-hydroxyapatite composite used for bone tissue engineering scaffold, Artif. Cells Blood Substit. Immobil. Biotechno. 31 (4) (2003) 435–448.

[64] H. Mutsuzaki, A. Kanamori, K. Ikeda, S. Hioki, T. Kinugasa, M. Sakane, Effect of calcium phosphate-hybridized tendon graft in anterior cruciate ligament reconstruction a randomized controlled trial, Am. J. Sports Med. 40 (8) (2012) 1772–1780.

[65] D. Amiel, C. Frank, F. Harwood, J. Fronek, W. Akeson, Tendons and ligaments: a morphological and biochemical comparison, J. Orthop. Res. : Off. Pub. Orthopaed. Res. Soc. 1 (3) (1984) 257–265.

[66] J. Apinun, S. Honsawk, S. Kuptniratsaikul, J. Jamkratoke, S. Kanokpanont, Osteogenic differentiation of rat bone marrow-derived mesenchymal stem cells encapsulated in Thai silk fibroin/collagen hydrogel: a pilot study in vitro, Asian Biomed. 12 (6) (2018) 273–279.

[67] L. Zhang, T. Yuan, L. Guo, X. Zhang, An in vitro study of collagen hydrogel to induce the chondrogenic differentiation of mesenchymal stem cells, J. Biomed. Mater. Res. 100A (10) (2012) 2717–2725.

[68] C. Hirzinger, M. Tauber, S. Korntner, M. Quirchmayr, H.-C. Bauer, A. Traweger, H. Tempfer, Acl injuries and stem cell therapy, Arch. Orthop. Trauma Surg. 134 (11) (2014) 1573–1578.

[69] D. Kouroupis, A. Kyrkou, E. Triantafyllidi, M. Katsimpoulas, G. Chalepakis, A. Goussia, A. Georgoulis, C. Murphy, T. Fotsis, Generation of stem cell-based bioartificial anterior cruciate ligament (acl) grafts for effective acl rupture repair, Stem Cell Res. 17 (2) (2016) 448–457.

[70] H. Liu, H. Fan, S.L. Toh, J.C.H. Goh, A comparison of rabbit mesenchymal stem cells and anterior cruciate ligament fibroblasts responses on combined silk scaffolds, Biomaterials 29 (10) (2008) 1443–1453.

[71] C. Kilmer, C.M. Battistoni, A. Cox, G.J. Breur, A. Panitch, J.C. Liu, Collagen type i and ii blend hydrogel with autologous mesenchymal stem cells as a scaffold for articular cartilage defect repair, ACS Biomater. Sci. Eng. 6 (6) (2020) 3464–3476.

[72] Y. Yao, P. Wang, X. Li, Y. Xu, G. Lu, Q. Jiang, Y. Sun, Y. Fan, X. Zhang, A di-self-crosslinking hyaluronan-based hydrogel combined with type i collagen to construct a biomimetic injectable cartilage-filling scaffold, Acta Biomater. 111 (2020) 197–207.
[73] W. Pan, Y. Wei, L. Zhou, D. Li, Comparative in vivo study of injectable biomaterials combined with bmp for enhancing tendon graft osteointegration for anterior cruciate ligament reconstruction, J. Orthop. Res. 29 (7) (2011) 1015–1021.
[74] A. Hassanzadeh, J. Ashrafihelan, R. Salehi, R. Rahbarghazi, M. Firouzamandi, M. Ahmadi, M. Khaksar, M. Alipour, M. Aghazadeh, Development and biocompatibility of the injectable collagen/nano-hydroxyapatite scaffolds as in situ forming hydrogel for the hard tissue engineering application, Artif. Cell Nanomed. Biotechnol. 49 (1) (2021) 136–146.
[75] V. Karageorgiou, D. Kaplan, Porosity of 3d biomaterial scaffolds and osteogenesis, Biomaterials 26 (27) (2005) 5474–5491.
[76] Y. Kuboki, Q.M. Jin, H. Takita, Geometry of carriers controlling phenotypic expression in bmp-induced osteogenesis and chondrogenesis, J. Bone Joint Surg. Am. 83A (2001) S105–S115.
[77] J. Gonzalez-Masis, J.M. Cubero-Sesin, S. Guerrero, S. Gonzalez-Camacho, Y. R. Corrales-Urena, C. Redondo-Gomez, J.R. Vega-Baudrit, R.J. Gonzalez-Paz, Self-assembly study of type i collagen extracted from male wistar hannover rat tail tendons, Biomater. Res. 24 (1) (2020) 19, 19.
[78] J.S. Temenoff, A.G. Mikos, Injectable biodegradable materials for orthopedic tissue engineering, Biomaterials 21 (23) (2000) 2405–2412.
[79] E.R. Garvican, M. Salavati, R.K.W. Smith, J. Dudhia, Exposure of a tendon extracellular matrix to synovial fluid triggers endogenous and engrafted cell death: a mechanism for failed healing of intrathecal tendon injuries, Connect. Tissue Res. 58 (5) (2017) 438–446.
[80] L. Sun, X. Zhou, B. Wu, M. Tian, Inhibitory effect of synovial fluid on tendon-to-bone healing: an experimental study in rabbits, Arthroscop. J. Arthroscop. Relat. Surg. 28 (9) (2012) 1297–1305.
[81] R.M. Delaine-Smith, G.C. Reilly, Mesenchymal stem cell responses to mechanical stimuli, Muscles, ligaments Tendons J. 2 (3) (2012) 169–180.
[82] S. Ishihara, S.M. Ponik, H. Haga, Mesenchymal stem cells in breast cancer: response to chemical and mechanical stimuli, Oncoscience 4 (11–12) (2017) 158–159.
[83] D.L. Butler, S.A. Goldstein, F. Guilak, Functional tissue engineering: the role of biomechanics, J. Biomech. Eng. Transact. Asme 122 (6) (2000) 570–575.
[84] C. Frank, The Science of Reconstruction of the Anterior Cruciate Ligament, 1997, p. 79.
[85] D. Greenwald, S. Shumway, P. Albear, L. Gottlieb, Mechanical comparison of 10 suture materials before and after in-vivo incubation, J. Surg. Res. 56 (4) (1994) 372–377.